

Highly Magnetizable Crosslinked Chloromethylated Polystyrene-Based Nanocomposite Beads for Selective Molecular Separation of 4-Aminobenzoic Acid

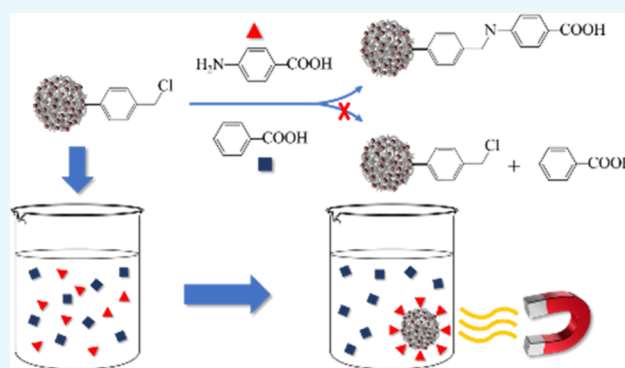
Fábio T. Costa,[†] Katiúscia V. Jardim,[†] Abraham F. Palomec-Garfias,[†] Paolin R. Cáceres-Vélez,[‡] Juliano A. Chaker,[†] Anderson M. M. S. Medeiros,[§] Sergio E. Moya,^{‡,†} and Marcelo H. Sousa^{*,†}

[†]Green Nanotechnology Group, Universidade de Brasília, Brasília DF 72220-900, Brazil

[‡]Soft Matter Nanotechnology Laboratory, CIC biomaGUNE, San Sebastián, Guip 20009, Spain

[§]Laboratoire de Chimie des Polymères Organiques, Université de Bordeaux, UMR5629, CNRS—Bordeaux INP—ENSCBP, 16 Avenue Pey-Berland, 33607 Pessac, Cedex, France

ABSTRACT: In this work, we describe the preparation and characterization of highly magnetizable chloromethylated polystyrene-based nanocomposite beads. For synthesis optimization, acid-resistant core–shelled maghemite ($\gamma\text{-Fe}_2\text{O}_3$) nanoparticles are coated with sodium oleate and directly incorporated into the organic medium during a suspension polymerization process. A crosslinking agent, ethylene glycol dimethacrylate, is used for copolymerization with 4-vinylbenzyl chloride to increase the resistance of the microbeads against leaching. X-ray diffraction, inductively coupled plasma atomic emission spectroscopy, thermogravimetric analysis, scanning electron microscopy, transmission electron microscopy, and optical microscopy are used for bead characterization. The beads form a magnetic composite consisting of ~ 500 nm-sized crosslinked polymeric microspheres, embedding ~ 8 nm $\gamma\text{-Fe}_2\text{O}_3$ nanoparticles. This nanocomposite shows large room temperature magnetization (~ 24 emu/g) due to the high content of maghemite (~ 45 wt %) and resistance against leaching even in acidic media. Moreover, the presence of superficial chloromethyl groups is probed by Fourier transform infrared and X-ray photoelectron spectroscopy. The nanocomposite beads displaying chloromethyl groups can be used to selectively remove aminated compounds that are adsorbed on the beads, as is shown here for the molecular separation of 4-aminobenzoic acid from a mixture with benzoic acid. The high magnetization of the composite beads makes them suitable for in situ molecular separations in environmental and biological applications.



1. INTRODUCTION

Magnetic microspheres have large potential for therapeutic and diagnostic applications in magnetically driven drug delivery, as contrast agents in magnetic resonance imaging, as devices for separation of biomolecules,¹ and in the environmental field as sorbents for removal of pollutants.² Among various types of nanocomposites, those designed by embedding magnetic nanoparticles (NPs) into a polymeric matrix stand out as ideal magnetic-hybrid and magneto-responsive materials, synergically combining the properties of the polymer matrix and the magnetic NPs.³ The polymer network provides mechanical stability and a large area for adsorption, whereas the inorganic nanoparticles bring magnetic responsivity. As a result, magnetic microspheres (or beads) show a high adsorptive capacity and can be rapidly and easily displaced by the application of an external magnetic field, replacing traditional forms of separation, such as centrifugation and filtration.⁴ In addition, since inorganic NPs encapsulated in the beads can generate heat through the interaction of their magnetic moments with an alternating magnetic field,

magnetic beads find applications in magnetic hyperthermia, both in the biomedical⁵ and environmental⁶ fields.

Magnetic polymer beads have additional characteristics that make them very appealing in the separation field. The polymeric matrix can be formed by different polymers that, besides encapsulating the magnetic NPs, bring the nanocomposites' functional groups, including groups for covalent coupling, and adsorption and affinity binding groups, necessary for the immobilization of molecules in the beads.¹ Covalent coupling is often desired for the immobilization of species on the nanocomposite surface, to keep them permanently bonded, not desorbing or leaching over time.⁷ Covalent coupling also brings specificity to the magnetic beads, since unwanted adsorbates, that may be attached nonspecifically or unbound to the surface, can be separated by successive washes/magnetic separations. Moreover, after magnetic separation, it is also

Received: January 15, 2019

Accepted: March 6, 2019

Published: March 21, 2019

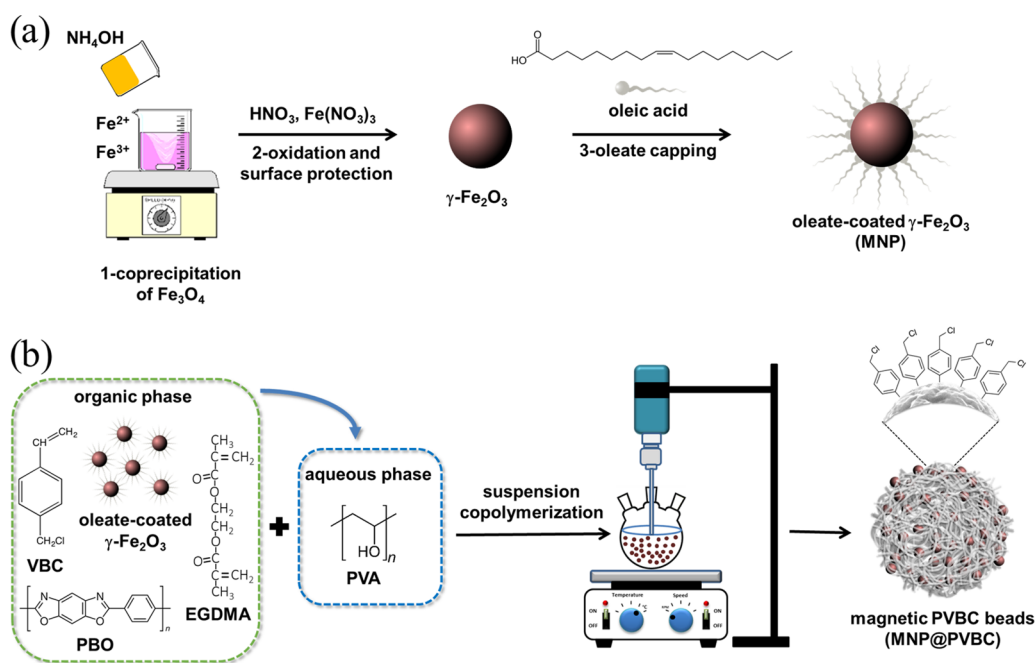


Figure 1. General scheme for the synthesis of oleate-capped $\gamma\text{-Fe}_2\text{O}_3$ NPs (a) and for the elaboration of magnetic PVBC beads (b).

possible to recover the adsorbate covalently bound to the nanocomposite surface through detaching/cleavage protocols.⁸

The continued interest in the development of new materials for trapping and separating molecules led us to propose the elaboration of a magnetic nanocomposite based on poly(4-vinylbenzyl chloride) (PVBC) microspheres embedding magnetic NPs. The vinylbenzyl chloride monomer (VBC) can be copolymerized with different monomers and displays the very reactive chloromethyl groups ($-\text{CH}_2\text{Cl}$) that retain their reactivity after polymerization, and can be covalently and reversibly bonded with a wide variety of organic moieties.⁹ Thus, PVBC acts as a polymeric support to carry out different reactions with multiple molecules, and after the molecular synthesis is completed, the covalently bound molecule can be separated from the chloromethyl group. Indeed, this material was the pioneer for the development of solid support resins for the synthesis of peptides—the Merrifield resin.¹⁰

Despite the potential applications of these materials, there are few reports on the elaboration of magnetic PVBC-based nanocomposites for separation and recovery of molecules. For instance, Rana and co-workers¹¹ prepared magnetic beads for solid-phase synthesis and reaction scavenging. In their process, magnetite particles were encapsulated within highly crosslinked polystyrene (chloromethyl styrene) through suspension polymerization. Darwish et al.¹² reported the elaboration of nanocomposites with this chlorine functionality, prepared by dispersion of oleate-coated magnetite nanoparticles on VBC by a multistep miniemulsion polymerization procedure. Using Fe_3O_4 , Chen and co-workers¹³ described the synthesis of a core–shelled magneto-polymeric materials through emulsion polymerization. The synthesized Fe_3O_4 @PVBC beads were successfully used for the enhancement of catalytic activity and stability of immobilized lipase by interfacial activation.

In our work, maghemite ($\gamma\text{-Fe}_2\text{O}_3$) NPs are chosen as the magnetic component of the nanocomposite, since they are more stable than magnetite, Fe_3O_4 (commonly employed for these purposes), and present relatively low toxicity and high saturation magnetization.¹⁴ Moreover, in the synthetic method

used, these NPs present a core–shell design with a thin surface layer that avoids dissolution of NPs in acidic medium.^{15,16}

Besides, our $\gamma\text{-Fe}_2\text{O}_3$ NPs were capped with oleate molecules, to improve their affinity to the organic phase during synthesis and guarantee a nanocomposite with a high charge of NPs homogeneously dispersed into the polymeric matrix.

We show here a cost-effective and potentially large-scale alternative by the direct incorporation of magnetic NPs into polystyrene beads by their inclusion into the polymerization mixture to produce a chloromethylated polystyrene-based nanocomposite with potential applications in the biomedical and environmental fields. The use of a simple suspension copolymerization method with an adequate crosslinking agent, associated with the hydrophobic-coated (and acid-resistant) $\gamma\text{-Fe}_2\text{O}_3$ NPs, led to a homogeneous nanocomposite with high magnetization saturation, not reported before, and high resistance against leaching even under acidic treatment. To test the potential of this nanocomposite to be used in selective separation of molecules through covalent coupling, a case study of selective adsorption was performed for the separation of 4-aminobenzoic acid (*p*-aminobenzoic acid, PABA) from a mixture with benzoic acid (BA). Particularly, PABA has been extensively applied in the dye stuff industry, pharmaceutical intermediates, and sunscreen. Therefore, developing efficient methods to separate and purify PABA is very important.¹⁷ Besides, this is a representative system of the potential of the nanocomposite for molecular separations since both acids have the same benzenecarboxylic acid backbone; nevertheless, the amino groups present only in PABA lead to its selective immobilization through covalent coupling with the superficial chloromethyl moieties of the nanocomposite. The work presented here proposes a strategy for the use of magnetic beads to selectively conjugate PABA that can be extended to other molecules by simple variation of coupling conditions and applied for selective molecule removal in environmental and biomedical applications.

2. MATERIALS AND METHODS

2.1. Materials. Iron(III) chloride hexahydrate ($\text{FeCl}_3 \cdot 6\text{H}_2\text{O}$); iron(II) chloride tetrahydrate ($\text{FeCl}_2 \cdot 4\text{H}_2\text{O}$); iron(III) nitrate nonahydrate ($\text{Fe}(\text{NO}_3)_3 \cdot 9\text{H}_2\text{O}$); nitric acid (HNO_3); oleic acid; the monomer, 4-vinylbenzyl chloride (VBC); the crosslinking agent, ethylene glycol dimethacrylate (EGDMA); the stabilizer, poly(vinyl alcohol) (PVA, $M_w = 125\,000$); and the initiator, benzoyl peroxide (PBO), were obtained from Sigma-Aldrich.

2.2. Sample Elaboration. The scheme of fabrication of the hybrid magnetic beads is shown in Figure 1. In a first step (Figure 1a), the elaboration of maghemite nanoparticles was carried out by following a procedure described elsewhere with a few modifications.¹⁸ Briefly, 125 mL of NH_4OH aqueous solution (2 mol/L) were quickly poured into 150 mL of aqueous solution containing 50 mmol of Fe^{3+} , 25 mmol of Fe^{3+} , and 20 mmol of HCl, under vigorous stirring (1000 rpm) at room temperature, for 60 min, to form a magnetite precipitate (Fe_3O_4). The precipitate was magnetically separated and washed with water several times until the solution reached neutral pH. Then, the NPs were acidified with HNO_3 (0.5 mol/L) and boiled with 0.5 mol/L $\text{Fe}(\text{NO}_3)_3$ for 30 min. This procedure was utilized both to oxidize magnetite to maghemite ($\gamma\text{-Fe}_2\text{O}_3$) and to create a layer rich in iron that protects the particles from acid dissolution.¹⁶ Finally, the precipitate was washed with acetone several times and dried at $\sim 60\text{ }^\circ\text{C}$. Then, maghemite NPs were functionalized with oleate molecules using a modification of a method described elsewhere.¹⁹ In a typical experiment, the synthesized maghemite NPs were dispersed into 200 mL of water, and the pH of the solution was adjusted to ~ 3 . After heating this solution until $80\text{ }^\circ\text{C}$, oleic acid (2 mL/g of $\gamma\text{-Fe}_2\text{O}_3$) was dropped at a rate of $\sim 1\text{ mL/min}$, and the mixture was stirred for 30 min. Within a few minutes, NPs were spontaneously transferred to the oily phase that, after cooling, was separated from the colorless water phase and washed five times with ethanol to remove water and excess surfactant, followed by drying at $60\text{ }^\circ\text{C}$. This sample will be referred to as MNP.

In a second step (Figure 1b), the preparation of the MNP-loaded PVBC composite was achieved by adopting a suspension polymerization procedure for nonmagnetic PVBC microbeads described elsewhere.²⁰ The details are as follows: 300 mg of as-prepared oleate-coated $\gamma\text{-Fe}_2\text{O}_3$ nanoparticles (MNP), 1.5 mL of EGDMA, 5.0 mL of VBC, and 0.12 g of PBO were well dissolved/dispersed in 7.5 mL of heptane. The resulting solution was dispersed in 80 mL of an aqueous PVA solution (3.2 g/L), and the polymerization was carried out at $80\text{ }^\circ\text{C}$ for 8 h, with the mechanical stirring rate kept constant at 800 rpm. After polymerization, the MNP-loaded PVBC composite (labeled MNP@PVBC) was washed exhaustively with ethanol, and then with water, to remove the diluent and unreacted monomer. Before the synthesis of our magnetic sorbent, we tested nanocomposites with different magnetic charges (25, 50, and 75 wt %). We found that nanocomposites with $\sim 50\text{ wt }%$ of magnetic material presented very high magnetization when compared to similar composites in the literature, easy separation by magnetic decantation, and preservation of the chemical functionalities of the polymer.

2.3. Sample Characterization. The size and morphology were evaluated by high-resolution transmission electron microscopy (TEM) using a JEM-2100 JEOL microscope and by field-emission scanning electron microscopy (FE-SEM)

using a Quanta 250 FEG. The particle size distribution was estimated from measuring about 300 particles (spherical shaped) found in an arbitrarily chosen area in enlarged images and using log-normal distribution. The crystalline structure of maghemite was analyzed by X-ray diffraction (XRD) in a Rigaku-Miniflex 600 diffractometer, with a radiation of 1.541 \AA (40 kV and 30 mA). Magnetization curves (at room temperature) were obtained in a magnetic field range of -20 to $+20\text{ kOe}$ using a vibrating sample magnetometer. Fourier transform infrared (FTIR) spectra were recorded with KBr pellets in the region of $4000\text{--}400\text{ cm}^{-1}$ on a Varian FTIR spectrophotometer with a resolution of 2 cm^{-1} . Thermogravimetric analysis (TGA) was conducted on a Shimadzu TG 60 thermogravimetric analyzer under a N_2 dynamic atmosphere ($50\text{ cm}^3/\text{min}$) in the temperature range of $35\text{--}600\text{ }^\circ\text{C}$, with a heating rate of $10\text{ }^\circ\text{C/min}$. The chemical composition was determined by Inductively coupled plasma atomic emission spectroscopy (ICP-OES) using an Optima 8000 DV ICP spectrometer, Perkin Elmer, in optical emission mode.²¹ X-ray photoelectron spectroscopy (XPS) experiments were performed on a SPECS Sage HR 100 spectrometer with a nonmonochromatic X-ray source (Mg $K\alpha$ line of 1253.6 eV energy and 250 W) and calibrated using the $3d_{5/2}$ line of Ag with a full-width at half-maximum (FWHM) of 1.1 eV. The selected resolution for the spectra was 15 eV of pass energy and 0.15 eV/step. All measurements were made in an ultra-high vacuum chamber at a pressure of around $8 \times 10^{-8}\text{ mbar}$. An electron flood gun was used to compensate for charging during XPS data acquisition. In the fittings, Gaussian–Lorentzian functions were used (after a Shirley background correction), where the FWHM of the peaks was constrained, whereas the peak positions and areas were set free. The peak position of each band was compared with the values available in the literature. The surface and pore-size distribution of outgassed samples were measured via N_2 adsorption at 77 K on a Micromeritics ASAP 2020 analyzer and using the Brunauer–Emmett–Teller (BET) model.

2.4. Batch Adsorption Experiments. Adsorption experiments were performed in conical tubes containing 100 mg of MNP@PVBC and 10 mL of PABA solution in the appropriate concentration. The flasks were placed in a Dubnoff orbital shaking water bath at $25\text{ }^\circ\text{C}$ and $\sim 200\text{ rpm}$. To evaluate the maximum adsorption capacity, the supernatant's initial and residual PABA concentrations were quantified using a Hitachi 3900 H UV–vis spectrometer in a quartz cell with a 1.0 cm optical path. Typical initial PABA concentrations ranged from 0 to 50 mg/L. To determine the minimum time required for adsorption to reach equilibrium, adsorption kinetic studies were carried out with an initial PABA concentration of 10 mg/L at $25\text{ }^\circ\text{C}$ and $\sim 200\text{ rpm}$. The concentrations of PABA were measured at different time intervals from 0 to 360 min.

The conventional kinetic models, pseudo-first-order and pseudo-second-order—expressed, respectively, as $q_t = q_e \ln(1 - \exp^{-k_1 t})$ and $q_t = \frac{k_2 q_e^2 t}{1 + k_2 q_e t}$ —were applied to analyze the experimental data of adsorption kinetics for a better understanding of the mechanism of adsorption.²² The rate constants of the pseudo-first-order and the pseudo-second-order models are, respectively, k_1 (1/min) and k_2 (g/(mg min)). The amount of adsorption at equilibrium, q_e (mg/g), can be calculated by $q_e = (C_0 - C_e) \frac{V}{m}$, where C_0 and C_e (mg/L) are the liquid-phase concentrations of the adsorbate initially and at

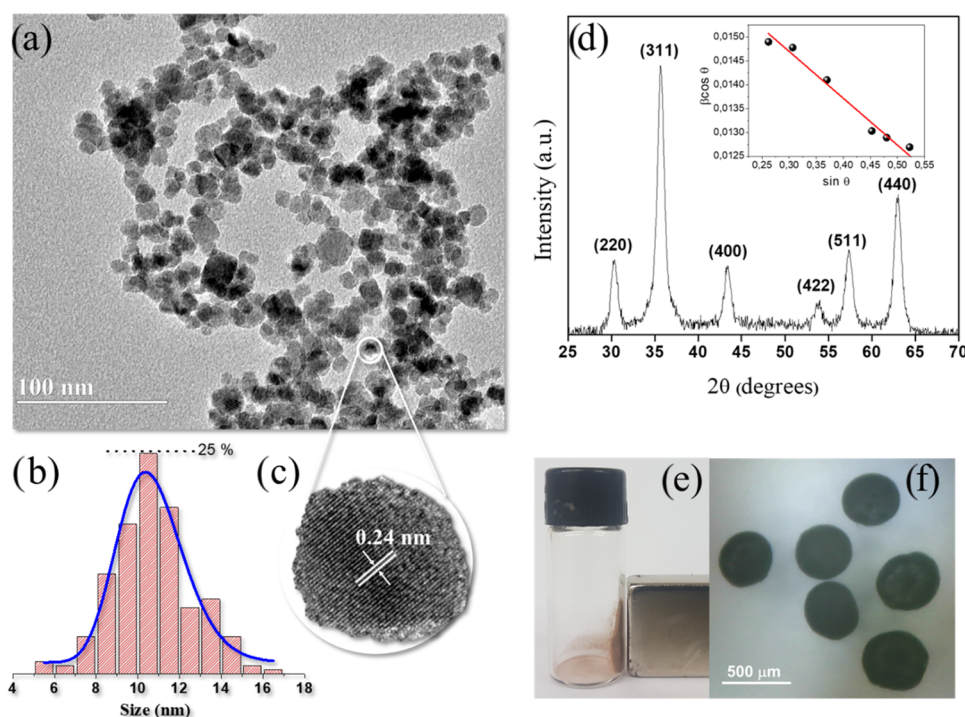


Figure 2. TEM image of γ -Fe₂O₃ NPs (a). Histogram of particle diameters: the solid line is the best fit using the log-normal size distribution (b). The lattice fringe of 0.24 nm corresponds to the (311) plane of γ -Fe₂O₃ (c). XRD pattern and Williamson–Hall plot (inset) of γ -Fe₂O₃ NPs (d). Magnetic nanocomposite (MNP@PVBC) under the action of a permanent magnet (e). Optical microscopy image of MNP@PVBC beads (f).

equilibrium, respectively, V is the volume of the solution (L), and m is the mass of the dry adsorbent used (g). The amount of adsorbate on the adsorbent at a time t , q_t (mg/g), is likewise calculated by $q_t = (C_0 - C_t) \frac{V}{m}$, where C_t (mg/L) is the liquid-phase concentration of the adsorbate at time t . To evaluate how the adsorbent and the adsorbate interact when the adsorption process reaches equilibrium, Langmuir and Freundlich classical isotherm models were applied.²³ In the Langmuir equation, $q_e = \frac{q_L C_e}{1 + k_L C_e}$, where q_L (mg/g) is the adsorption capacity of the adsorbent and k_L (L/mg) is the Langmuir constant, which is related to the affinity of the binding sites. The Freundlich equation is described as $q_e = K_F C_e^{1/n}$, where K_F is the Freundlich isotherm constant and $1/n$ is the heterogeneity factor.

3. RESULTS AND DISCUSSION

In the TEM image of oleate-coated γ -Fe₂O₃ nanoparticles (MNP) shown in Figure 2a, NPs present a nearly spherical morphology and are polydisperse in size. The average diameter and polydispersity index were 10.6 nm and 0.22, respectively, and were calculated from the histogram in Figure 2b. Furthermore, the lattice fringes (0.24 nm) in Figure 2c agree well with the distance between the (311) lattice planes of the maghemite structure. The XRD pattern of the oleate-coated γ -Fe₂O₃ sample is shown in Figure 2d. All peaks could be readily indexed to a face-centered cubic spinel structure ($Fd\bar{3}m$) of maghemite, and the calculated lattice parameter (0.83488 nm), obtained from the literature (JCPDS #39-1346). Moreover, the crystallite size ($d_{XRD} = 8.7$ nm) and strain ($\epsilon = 4.9 \times 10^{-3}$) were, respectively, obtained from the intercept on the y -axis and the slope of the line on the Williamson–Hall

plot (inset of Figure 2d), through the equation $\beta \cos \theta = 0.94\lambda/d_{XRD} + 2\epsilon \sin \theta$, where λ is the wavelength of X-rays, β is the broadening of the diffraction peak measured at half of its maximum intensity, and θ is Bragg's diffraction angle.²⁴

Figure 2e shows the MNP@PVBC composite under the action of a permanent magnet. In the image, it can be seen that the hybrid beads with the magnetic NPs resulted in a macroscopic homogeneous magnetizable material. Moreover, as shown by optical micrography of the MNP@PVBC composite (see Figure 2f), fairly uniform spherical micro-particles with sizes $\sim 500 \mu\text{m}$ were formed during polymerization.

As shown in the SEM image of Figure 3a, the magnetic PVBC beads possess a relatively uniform rough surface. In the highly magnified image in Figure 3b, the presence of numerous pores can be recognized. The authors ascribe the presence of pores in polymer matrixes to the possible presence of amphiphilic, partially hydrolyzed polymer that is able to trap water, stabilizing it inside the oil droplets and resulting in the formation of pores.²⁵ Moreover, a porous structure can allow the easy penetration of reagents, especially in the presence of swelling solvents,¹⁰ which can be useful for the application of nanocomposite as solid support for organic reactions and magnetic separations. Higher magnified images of MNP@PVBC (see Figure 3c) show that γ -Fe₂O₃ NPs are trapped on the surface and inside of the pores of the PVBC beads. Moreover, a TEM image of an internal slice of the MNP@PVBC sample (Figure 3d) indicates that γ -Fe₂O₃ NPs are also embedded into the polymer core (light-gray part). The composite beads display a surface area of $\sim 320 \text{ m}^2/\text{g}$ and pore volume of $\sim 0.085 \text{ cm}^3/\text{g}$, as obtained from BET (see Figure 3e), and these results corroborate the SEM measurements. Large superficial area and small pore diameter could be

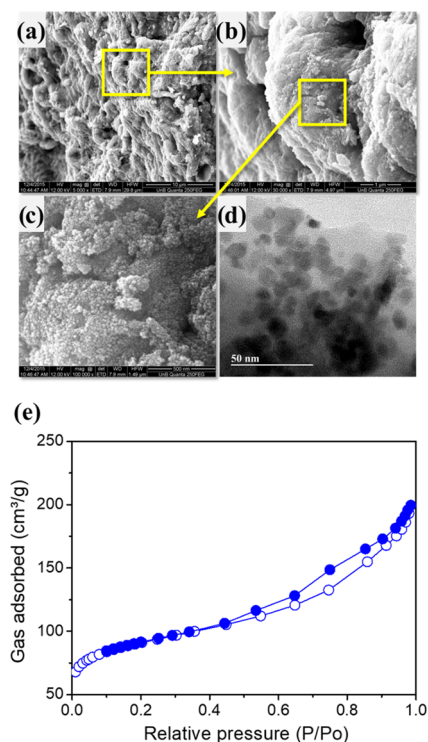


Figure 3. Scanning electron micrographs of the magnetic nanocomposite (MNP@PVBC) at 5000 \times (a), at 30 000 \times (b) and at 100 000 \times (c) magnification. TEM image of an internal slice of the MNP@PVBC sample (d). N₂ adsorption (solid points) and desorption (hollow points) isotherms of MNP@PVBC (e).

also due to the presence of nanosized particles, respectively, at the surface and in the pores of the polymer structures.

Thermogravimetric analysis was used for the estimation of the mass percentage of magnetic NPs on the nanocomposite. Most of the loss of mass presented by the multistage weight loss profile of the MNP@PVBC composite (see Figure 4a) can be attributed to the thermal decomposition of the polymeric/organic counterpart and eventually free and chemically adsorbed water.²⁶ In the case of oleate-coated NPs, the weight loss must be mostly due to the adsorbed oleate capping.²⁷ The magnetic content (in terms of γ -Fe₂O₃ wt %) determined from TGA data for MNP and MNP@PVBC samples were, respectively, \sim 16 and 55%.

Magnetization measurements were also performed to evaluate the counterparts of the polymeric phase in the magnetic properties of the nanocomposite. Figure 4b shows the room temperature magnetization as a function of the applied magnetic field for the oleate-capped γ -Fe₂O₃ (MNP) and MNP@PVBC nanocomposite. The saturation magnetization (M_s) of the MNP sample, determined at the maximum applied magnetic field, was \sim 50.7 emu/g and was found to be lower than the bulk magnetization of maghemite (\sim 80 emu/g).²⁸ This decrease can be caused by the surface coordination,²⁹ cationic redistribution,³⁰ and surface and finite size effects,^{31,32} which affect the magnetic properties of nanosized grains. Moreover, nanoparticles show superparamagnetic-like behavior, with negligible remanence and coercivity. After polymerization, the saturation magnetization of the nanocomposite decreased to \sim 24.3 emu/g, supporting the claim that magnetic NPs are embedded in a “nonmagnetic” polymeric matrix to form a multicore system. If one assumes

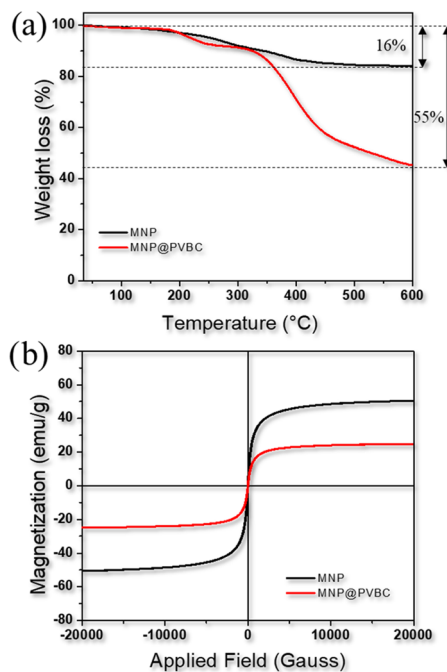


Figure 4. Thermograms (a) and magnetization curves (b) obtained for the oleate-capped γ -Fe₂O₃ NPs (MNP) and magnetic nanocomposite (MNP@PVBC).

that the magnetic core is preserved after dispersion into the polymeric matrix, the extent of the decrease in M_s can be associated with the amount of polymeric material around the NPs.³³ Then, the amount of magnetic material can be estimated to be \sim 47.9% in mass, slightly lower than that determined from TGA measurements. Besides, the dosage of iron on the MNP@PVBC sample using ICP-OES allowed estimating a magnetic content of \sim 44.5 wt % in γ -Fe₂O₃, in close agreement with the magnetization data.

Figure 5 shows the FTIR spectra of the MNP and MNP@PVBC samples. The spectrum of PVBC blank beads,

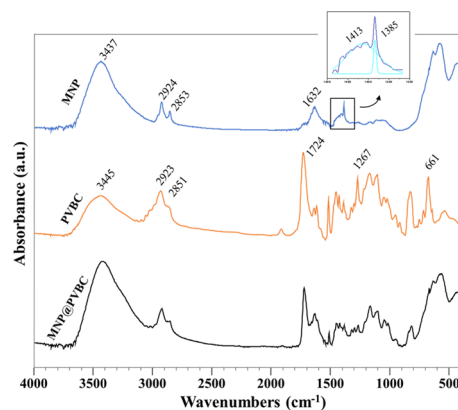


Figure 5. FTIR spectrum of the magnetic nanocomposite (MNP@PVBC) compared to their respective constituents.

synthesized as described for the MNP@PVBC sample in the Materials and Methods section, but without γ -Fe₂O₃ NPs, is also shown in this graph for comparison purposes. The main vibration bands were depicted with the intention of helping in probing the architecture of the nanocomposite. In the spectrum of oleate-capped maghemite NPs, the broad

structure below 800 cm^{-1} can be attributed to Fe–O vibrations of the crystalline lattice of nanocrystalline $\gamma\text{-Fe}_2\text{O}_3$.¹⁵ The intense peak at $\sim 1385\text{ cm}^{-1}$ could be due to adsorbed NO_3^- ions during the synthesis of iron oxide (see peak deconvolution in the inset), and the characteristic bands of –OH appeared at 3437 cm^{-1} , which was probably due to water adsorption on the NP's surface.¹⁴ The asymmetric CH_2 stretch and the symmetric CH_2 stretch from the oleic acid backbone appear at 2924 and 2853 cm^{-1} , respectively.³⁴ Also, the carbonyl vibrations of free oleic acid (normally at $\sim 1710\text{ cm}^{-1}$) are absent in this sample and replaced by the asymmetric and symmetric stretching vibrations of carboxyl ($-\text{COO}^-$) at 1632 and 1413 cm^{-1} , indicating that the oleic acid is chemisorbed on the nanoparticles' surface through iron metal carboxylate coordination.³⁴

This is a crucial condition for the successful synthesis of the magnetic PVBC beads, since the $\gamma\text{-Fe}_2\text{O}_3$ NPs after coprecipitation have a polar surface⁶ and thus are not able to disperse into the polymeric matrix. After oleate grafting, the NP's surface becomes hydrophobic and can be dispersed into the organic phase and homogeneously trapped into the polymer body during polymerization.²⁷ In the pure PVBC FTIR spectrum, the broad band at 3441 cm^{-1} (O–H stretching vibration) also suggests the presence of adsorbed water on the polymer and possibly the presence of PVA utilized in the synthesis.¹³ The C–H stretching vibrations with absorption bands between 2924 and 2853 cm^{-1} also appear, indicating the presence of PVA and EGDMA components. The absorption bands corresponding to the aromatic ring with disubstituted $\text{C}=\text{C}$ appear between 1440 and 1640 cm^{-1} , confirming the formation of PVBC.¹² Moreover, the carbonyl stretch of EGDMA falls at 1724 cm^{-1} , and the absorptions for the C–Cl bond at 1267 and 661 cm^{-1} can be seen, confirming the presence of chloromethyl groups on the microbeads' surface.³⁵

The main vibrations observed in the spectra of pure PVBC and those of oleate-coated $\gamma\text{-Fe}_2\text{O}_3$ NPs are still present in the spectrum of magnetic PVBC beads (sample MNP@PVBC), confirming the presence of inorganic NPs embedded into the polymeric matrix. Moreover, the slight dislocation of some bands, when compared with pure components, indicates the interaction between inorganic and organic polymeric phases.

The XPS spectra of Fe 2p, C 1s, Cl 2p and O 1s core levels in Figure 6 give additional proof of the chemical structure and surface composition of the microbeads. More specifically, in the Fe 2p core-level spectrum of the MNP@PVBC sample (Figure 6a), the Fe ($2p_{3/2}$) and Fe ($2p_{1/2}$) peaks appear at about 711.7 and 725.2 eV , respectively, indicating that iron is fully oxidized and magnetic NPs are composed of maghemite.³⁶ Indeed, this Fe ($2p_{3/2}$) peak is a characteristic of the core-level electrons, whereas the Fe ($2p_{1/2}$) peak can be attributed to the carboxylate–Fe bond.³⁷ The large peak in the C 1s core-level spectrum of the MNP@PVBC surface (Figure 6b) is ascribed to the convolution of the C–H/C–C, C–O/C–Cl, and $\text{O}=\text{C}-\text{O}$ species, with components centered at about 284.6 , 286.3 , and 288.5 eV , confirming the formation of the PVBC structure and the presence of the oleate coating.²⁰

Moreover, the contribution of the $\text{O}=\text{C}-\text{O}$ component in the fitted curve also indicates a successful crosslinking of EGDMA in the copolymer. Besides, the absence of the C 1s peak corresponding to carboxylic carbon ($-\text{COOH}$), normally posited at 290 eV , indicates the absence of free oleic acid on the coated $\gamma\text{-Fe}_2\text{O}_3$ NPs.³⁷ The O 1s spectrum in Figure 6c is

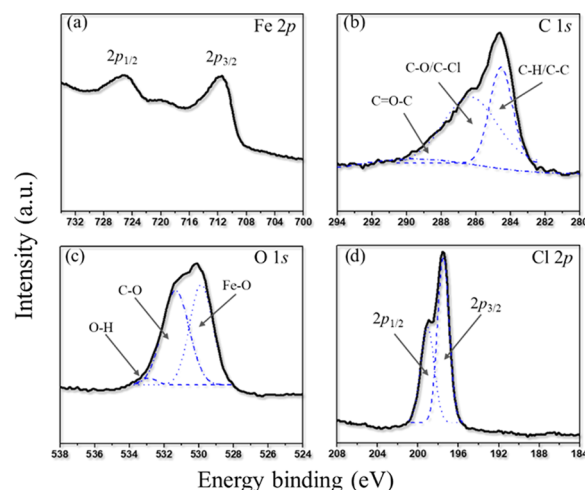


Figure 6. Fe 2p (a), C 1s (b), O 1s (c) and Cl 2p (d) core-level XPS spectra of the magnetic nanocomposite (MNP@PVBC).

deconvoluted into three peaks at binding energies of about 533.1 , 531.4 , and 529.9 eV , respectively, corresponding to –OH, C–O, and Fe–O moieties,³⁸ reinforcing the successful embedding of oleate-coated maghemite NPs into the body of the crosslinked copolymer. Moreover, as shown in Figure 6d, the Cl 2p core-level spectrum of the MNP@PVBC sample consists of the Cl ($2p_{3/2}$) and Cl ($2p_{1/2}$) doublet centered at about 199.7 and 197.5 eV , respectively, attributable to the covalently bonded chlorine (C–Cl) species, thus confirming the presence of chloromethyl moieties on the nanocomposite surface.²⁰

The leaching of magnetic NPs and iron from the beads was investigated by stirring the MNP@PVBC sample for 60 min in water at $\text{pH} \sim 7$. After magnetic separation, the analysis of the supernatant using ICP-OES showed that the NPs were stably incorporated into the polymer core. Treatment of the nanocomposite in a similar way with 0.1 mol/L NaOH , 0.1 mol/L HCl , and trifluoroacetic acid (25%) resulted in low levels of iron in solution ($< 100\text{ }\mu\text{g/L}$). Since iron leaching was not observed even under acidic treatment, and also from the cross-analysis of XRD, microscopy, magnetization, TGA, and ICP-OES results substantiated with the FTIR and XPS data, we can conclude that we have produced a copolymer of PVBC crosslinked with EGDMA and firmly trapped $\gamma\text{-Fe}_2\text{O}_3$ NPs, forming a homogeneous magnetic nanocomposite. The high chemical stability of the core-designed magnetic $\gamma\text{-Fe}_2\text{O}_3$ NPs also must have contributed to the resistance of the nanocomposite against dissolution.

Besides, a chloromethylated material with a large amount of $-\text{CH}_2\text{Cl}$ functional groups bonded to the microbeads' surface was produced. In fact, the availability of $-\text{CH}_2\text{Cl}$ groups on the nanocomposite surface was assessed by a simple test, as shown in Figure 7a. After synthesis, due to the presence of chloromethyl groups on the surface, the nanocomposite has a hydrophobic character and is poorly dispersible in water. After mixing with ammonium hydroxide (2.0 mol/L), amination of superficial chloromethyl groups occurs and dispersion of the nanocomposite is easier in aqueous solution, due to the more hydrophilic $-\text{CH}_2\text{NH}_2$ groups, formed after the reaction.¹³

To evaluate the potential of this nanocomposite to be used in selective separation of molecules through covalent coupling, a case study of selective adsorption was performed for the separation of 4-aminobenzoic acid (PABA) from a mixture

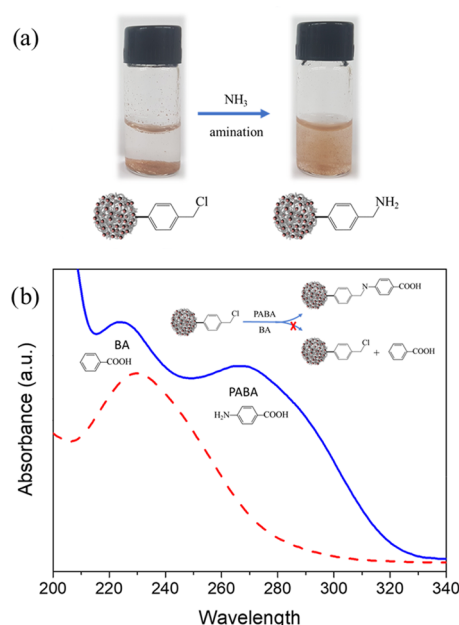


Figure 7. (a) Dispersibility of the nanocomposite after vortexing and resting 30 s, before amination (left) and after amination (right) with concentrated NH₄OH. (b) UV-vis spectra of a benzoic acid (BA) and 4-aminobenzoic acid (PABA) mixture, before interaction (blue full line) and after interaction (red dashed line) with the MNP@PVBC nanocomposite. The inset shows a reaction scheme of MNP@PVBC with BA and PABA.

with benzoic acid (BA). In a qualitative test, beads were suspended in a solution of benzoic acid (BA) and 4-aminobenzoic acid (or *p*-aminobenzoic acid, PABA), 10 mg/L at pH \sim 7 for 60 min under magnetic stirring. Then, the beads were separated magnetically with a permanent magnet, and the supernatant was analyzed using UV-vis spectroscopy. As shown in the spectra of Figure 7b, the characteristic absorbance of PABA at \sim 268 nm decreased substantially, whereas the absorbance of BA at \sim 230 nm was only slightly reduced after interaction with magnetic microbeads. The decrease in the absorbance of PABA is due to the nucleophilic reaction of $-NH_2$ groups of PABA with the chloromethyl moieties of the nanocomposite. Then, the covalently bonded PABA is removed together with the beads during magnetic separation. However, BA is not removed as its carboxylic group does not form a covalent linkage with chloromethyl under these experimental conditions.³⁹ This qualitative test hints that the magnetic beads could be applied to selectively conjugate different molecules by a simple variation of coupling conditions and applied for selective molecule removal.

Batch mode kinetics and isotherm studies were also carried out to evaluate the performance of our beads and gain insight into the mechanisms involved in the selective adsorption. Figure 8 shows the effect of contact time on the adsorption of PABA and BA by magnetic sorbents. The adsorption capacity of PABA (black spheres) quickly increased until \sim 100 min and then slowly until the adsorption equilibrium was reached within $t > 120$ min. Otherwise, the constant and low adsorption capacity of BA (gray spheres) indicates this acid was not efficiently adsorbed by the nanosorbents even at longer times. The kinetic parameters and correlation coefficients obtained from data fitting using the models described in the experimental part, for PABA adsorption, are

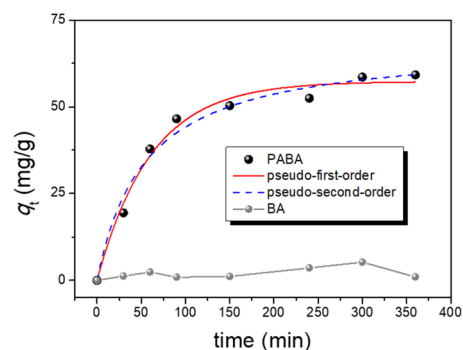


Figure 8. Effect of contact time on the adsorption of PABA (black spheres) and BA (gray spheres) by the MNP@PVBC magnetic sorbent. The dashed line is the pseudo-first-order model simulation; the solid line is the pseudo-second-order model simulation.

summarized in Table 1. The pseudo-second-order kinetic model best fits the adsorption of PABA. Indeed, the R^2

Table 1. Kinetics and Isotherm Parameters for the Adsorption of PABA by Magnetic Sorbents

kinetics parameters	
pseudo-first-order	pseudo-second-order
$R^2 = 0.979$	$R^2 = 0.984$
$k_1 = 0.017$ (1/min)	$k_2 = 2.69$ (g/(mg min))
$q_e = 56.2$ (mg/g)	$q_e = 68.0$ (mg/g)
adsorption parameters	
Langmuir	Freundlich
$R^2 = 0.995$	$R^2 = 0.901$
$k_L = 0.78$ (L/mg)	$n = 4.1$
$q_L = 66.2$ (mg/g)	$q_F = 68.0$ (mg/g)

coefficient for the pseudo-second-order model slightly exceeded that of the pseudo-first-order model. Furthermore, the adsorption capacity extrapolated from the graph is in better accordance with the adsorption capacity obtained from the pseudo-second-order model than that obtained using the pseudo-first-order kinetic model. On the basis of the above result, a contact time of 120 min was selected for ensured establishment of the adsorption equilibrium in further adsorption studies.

As shown in Figure 9, the adsorption isotherm of PABA in MNP@PVBC showed a nonlinear shape over a wide range of PABA concentrations. The adsorption capacity of the magnetic sorbent increased with increasing equilibrium concentration of PABA, tending to reach saturation progressively. The simulated curves using Langmuir and Freundlich equations are also plotted in the graph of Figure 9, and their calculated parameters are listed in Table 1. The Langmuir adsorption isotherm assumes that ideal adsorption occurs at a fixed number of finite and identical localized surface sites, with each site holding one adsorbate molecule, forming a monolayer, and no subsequent interaction between adsorbed species. Otherwise, the Freundlich model is an empirical model for heterogeneous systems which describes reversible adsorption not restricted to the formation of a monolayer.²³ The Langmuir correlation coefficient is much higher than that of the Freundlich isotherm, indicating that Langmuir is the best fit model, and there is a tendency to form a PABA monolayer on the sorbent surface. These results corroborate the proposed

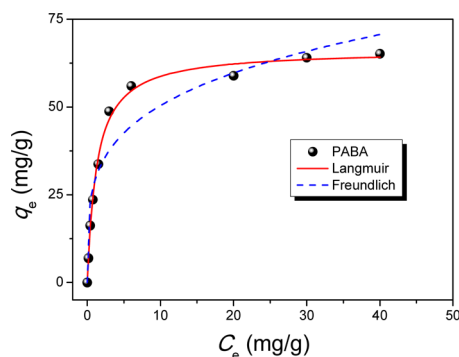


Figure 9. Adsorption isotherms of PABA (black spheres) by the MNP@PVBC magnetic sorbent. The solid line corresponds to the Langmuir model simulation; the dotted line is the Freundlich model simulation.

model of molecular adsorption of amino moieties from PABA by the chloromethyl groups on the surface of the magnetic sorbent. Once $-\text{CH}_2\text{Cl}$ superficial sites are occupied by PABA (forming a monolayer), the adsorption decreases, since no more chloromethyl groups are available to form successive layers of adsorption. Moreover, in the interval of C_0 investigated, the separation factor parameter $R_L = \frac{1}{1 + k_1 C_0}$ lies between ~ 0.03 and ~ 0.9 , indicating a favorable condition for adsorption, thus suggesting the applicability of this magnetic sorbent for PABA removal from a mixture with BA.

Compared with other similar materials in the limited available literature, we apply a simple methodology leading to a homogeneous nanocomposite with a high magnetization saturation, not reported before, and a high resistance against leaching even under acidic treatment. For instance, magnetite particles were encapsulated within highly crosslinked polystyrene (chloromethyl styrene) through suspension polymerization.¹¹ These microbeads presented resistance against iron leaching in acid media; however, the magnetization was very small with a resin containing ~ 0.6 wt % of magnetic material. Magnetic nanocomposites with this chlorine functionality were also prepared by dispersion of oleate-coated magnetite nanoparticles on VBC by a multistep miniemulsion polymerization procedure.¹² In this process, the material contained 1–2 wt % of magnetic material and presented some leaching of iron in the presence of concentrated acids.

To the best of our knowledge, there has been no report on the preparation of chloromethylated magnetic beads for PABA for the removal of aminated compounds. Besides, a few reports deal with the preparation of similar chloromethyl functionalized polymeric beads for the removal of other adsorbate species. These works mainly take advantage of the ability of $-\text{CH}_2\text{Cl}$ to follow click reactions for tuning the surface functionality of beads, increasing their specific adsorptive capacity for a given species. For instance, Lapwanit et al.⁴⁰ prepared chelating magnetic copolymer beads, based on poly(vinylbenzyl chloride-*co*-styrene-*co*-divinylbenzene), by click attachment with propargyl alcohol via triazole formation. This surface chemical functionality allowed metal chelate adsorption, for Zn(II), Cu(II), and Ni(II), with adsorption capacities of about 67, 61, and 57 mg/g, respectively.

Our composite beads showed good performance, in view of adsorptive assays for PABA, when compared with other nonmagnetic beads. Wang et al.¹⁷ showed the preparation of a chloromethylated poly(styrene-*co*-divinylbenzene) hyper-

crosslinked resin, modified with formaldehyde carbonyl, quinone carbonyl, and phenolic hydroxyl groups, for the adsorption of PABA. The authors found that the isotherms followed the Langmuir model, with an adsorption kinetics that could be characterized by a pseudo-second-order rate equation, and that the formation of hydrogen bonding between the surface groups and PABA was one of the primary driving forces for the adsorption. The authors reported an adsorption capacity of ~ 75 mg/g (and equilibrium times >100 min) for PABA. Yu et al.⁴⁰ produced L-malic acid-modified hypercrosslinked resins, synthesized from a macroporous chloromethylated styrene–divinylbenzene copolymer by Friedel–Crafts reaction and esterification reaction for PABA adsorption. The authors associated the optimal adsorption capacity (>200 mg/g) of beads with hydrogen bonding driving force and hydrophilicity enhancement. Besides, kinetic curves were characterized by a pseudo-second-order rate equation (equilibrium time ~ 200 min), and the isotherms could be fitted by the Langmuir model.

We believe that the good performance of our beads is because PABA is covalently linked to the polymer matrix, which is more effective in removing PABA from solution. Moreover, the high magnetization of the composite beads makes them suitable for in situ molecular separations in environmental and biological applications.

4. CONCLUSIONS

In this work, we have demonstrated an effective strategy for the fabrication of chloromethylated polystyrene-based magnetic nanocomposite beads. The beads displayed a high saturation magnetization, due to the large amount of magnetic material, and improved resistance against acidic dissolution, thanks to the crosslinking and the presence of core–shelled magnetic NPs. Moreover, high loading of chloromethyl groups and high accessibility of the reactive sites for selective coupling of molecules were demonstrated. Chloromethyl groups can be used for selective coupling of molecules from solutions with several molecules, and the coupled molecules will be then magnetically removed from solution with the beads. We showed here that aminated compounds can be selectively removed from molecular mixtures by means of the magnetic composite beads. Based on the results, the nanocomposite fabricated in this work demonstrated large potential to be used as a tool for selective removal of pollutants from contaminated water through magnetically assisted covalent separation. Applications such as magnetic solid supports for the separation, immobilization, or synthesis of biomolecules in the biomedical field could also be considered for this material. A very important result from this work is that it is possible to obtain composite polymer beads with a magnetization not higher than that reported in the literature for similar polymer chemistry. The high magnetization of the beads ensures that they can be recovered applying a magnetic field, which makes them suitable for in situ applications, where other methodologies for separation are not possible.

■ AUTHOR INFORMATION

Corresponding Author

*E-mail address: mhsqui@gmail.com. Phone: +55 61 992060946.

ORCID

Sergio E. Moya: 0000-0002-7174-1960

Marcelo H. Sousa: 0000-0003-1210-8329

Notes

The authors declare no competing financial interest.

ACKNOWLEDGMENTS

The authors gratefully acknowledge financial support from Brazilian Agencies: Conselho Nacional de Desenvolvimento Científico e Tecnológico (CNPq), Coordenação de Aperfeiçoamento de Pessoal de Nível Superior (CAPES), Fundação de Apoio à Pesquisa do Distrito Federal (FAPDF), Decanato de Pesquisa e Inovação (DPI-UnB), and Fundação de Empreendimentos Científicos e Tecnológicos (FINATEC). The authors also thank LabMic-UFG for TEM measurements. S.E.M. thanks the MAT2017-88752-R Retos project from the Ministerio de Economía, Industria y Competitividad, gobierno de España.

REFERENCES

- (1) Philippova, O.; Barabanova, A.; Molchanov, V.; Khokhlov, A. Magnetic Polymer Beads: Recent Trends and Developments in Synthetic Design and Applications. *Eur. Polym. J.* **2011**, *47*, 542–559.
- (2) Ngomsik, A.; Bee, A.; Draye, M.; Cote, G.; Cabuil, V. Magnetic Nano- and Microparticles for Metal Removal and Environmental Applications: A Review. *C. R. Chim.* **2005**, *8*, 963–970.
- (3) Gervald, A. Y.; Gritskova, I. A.; Prokopov, N. I. Synthesis of Magnetic Polymeric Microspheres. *Russ. Chem. Rev.* **2010**, *79*, 219–229.
- (4) Borlido, L.; Azevedo, A. M.; Roque, A. C. A.; Aires-Barros, M. R. Magnetic Separations in Biotechnology. *Biotechnol. Adv.* **2013**, *31*, 1374–1385.
- (5) Kafrouni, L.; Savadogo, O. Recent Progress on Magnetic Nanoparticles for Magnetic Hyperthermia. *Prog. Biomater.* **2016**, *5*, 147–160.
- (6) Rodovalho, F. L.; Capistrano, G.; Gomes, J. A.; Sodré, F. F.; Chaker, J. A.; Campos, A. F. C.; Bakuzis, A. F.; Sousa, M. H. Elaboration of Magneto-Thermally Recyclable Nanosorbents for Remote Removal of Toluene in Contaminated Water Using Magnetic Hyperthermia. *Chem. Eng. J.* **2016**, *302*, 725–732.
- (7) Siiman, O.; Burshteyn, A.; Insausti, M. E. Covalently Bound Antibody on Polystyrene Latex Beads: Formation, Stability, and Use in Analyses of White Blood Cell Populations. *J. Colloid Interface Sci.* **2001**, *234*, 44–58.
- (8) Yajima, H.; Fuhii, N.; Funakoshi, S.; Watanabe, T.; Murayama, E.; Otaka, A. New Strategy for the Chemical Synthesis of Proteins. *Tetrahedron* **1988**, *44*, 805–819.
- (9) Thunhorst, K. L.; Noble, R. D.; Bowman, C. N. Preparation of Functionalized Polymers by Reactions of Poly(Vinylbenzyl Chloride). *Polymer Modification*; Springer: Boston, MA, 1997; pp 97–107.
- (10) Merrifield, R. B. Solid Phase Peptide Synthesis. I. The Synthesis of a Tetrapeptide. *J. Am. Chem. Soc.* **1963**, *85*, 2149–2154.
- (11) Rana, S.; et al. Synthesis of Magnetic Beads for Solid Phase Synthesis and Reaction Scavenging. *Tetrahedron Lett.* **1999**, *40*, 8137–8140.
- (12) Darwish, M. S. A.; MacHunsky, S.; Peuker, U.; Kunz, U.; Turek, T. Magnetite Core-Shell Nano-Composites with Chlorine Functionality: Preparation by Miniemulsion Polymerization and Characterization. *J. Polym. Res.* **2011**, *18*, 79–88.
- (13) Chen, Z.; Liu, L.; Yang, R. Improved Performance of Immobilized Lipase by Interfacial Activation on Fe₃O₄@PVBC Nanoparticles. *RSC Adv.* **2017**, *7*, 35169–35174.
- (14) Palomec-Garfias, A. F.; Jardim, K. V.; Sousa, M. H.; Márquez-Beltrán, C. Influence of Polyelectrolyte Chains on Surface Charge and Magnetization of Iron Oxide Nanostructures. *Colloids Surfaces A Physicochem. Eng. Asp.* **2018**, *549*, 13–24.
- (15) Sousa, M. H.; Tourinho, F. A.; Rubim, J. C. Use of Raman Micro-Spectroscopy in the Characterization of M(II)Fe₂O₄ (M = Fe, Zn) Electric Double Layer Ferrofluids. *J. Raman Spectrosc.* **2000**, *31*, 185–191.
- (16) Gomes, J. D. A.; Sousa, M. H.; Tourinho, F. A.; Aquino, R.; Da Silva, G. J.; Depeyrot, J.; Dubois, E.; Perzynski, R. Synthesis of Core-Shell Ferrite Nanoparticles for Ferrofluids: Chemical and Magnetic Analysis. *J. Phys. Chem. C* **2008**, *112*, 6220–6227.
- (17) Wang, X.; Huang, J.; Huang, K. Surface Chemical Modification on Hyper-Cross-Linked Resin by Hydrophilic Carbonyl and Hydroxyl Groups to Be Employed as a Polymeric Adsorbent for Adsorption of p-Aminobenzoic Acid from Aqueous Solution. *Chem. Eng. J.* **2010**, *162*, 158–163.
- (18) Coelho, B. C. P.; Siqueira, E. R.; Ombredane, A. S.; Joanitti, G. A.; Chaves, S. B.; Silva, S. W.; Chaker, J. A.; Longo, J. P. F.; Azevedo, R. B.; Morais, P. C.; et al. Maghemite-gold core-shell nanostructures (γ -Fe₂O₃@Au) surface-functionalized with aluminium phthalocyanine for multi-task imaging and therapy. *RSC Adv.* **2017**, *7*, 11223–11232.
- (19) Lam, T.; Avti, P. K.; Pouliot, P.; Maafi, F.; Tardif, J.; Rhéaume, É.; Lesage, F.; Kakkar, A. Fabricating Water Dispersible Superparamagnetic Iron Oxide Nanoparticles for Biomedical Applications through Ligand Exchange and Direct Conjugation. *Nanomaterials* **2016**, *6*, No. 100.
- (20) Cheng, Z.; Zhu, X.; Shi, Z. L.; Neoh, K. G.; Kang, E. T. Polymer Microspheres with Permanent Antibacterial Surface from Surface-Initiated Atom Transfer Radical Polymerization. *Ind. Eng. Chem. Res.* **2005**, *44*, 7098–7104.
- (21) Sousa, M. H.; Geraldo, J.; Depeyrot, J.; Tourinho, F. A.; Zara, L. F. Chemical Analysis of Size-Tailored Magnetic Colloids Using Slurry Nebulization in ICP-OES. *Microchem. J.* **2011**, *97*, 182–187.
- (22) Kumar, K. V. Linear and Non-Linear Regression Analysis for the Sorption Kinetics of Methylene Blue onto Activated Carbon. *J. Hazard. Mater.* **2006**, *137*, 1538–1544.
- (23) Foo, K. Y.; Hameed, B. H. Insights into the Modeling of Adsorption Isotherm Systems. *Chem. Eng. J.* **2010**, *156*, 2–10.
- (24) Mote, V. D.; Purushotham, Y.; Dole, B. N. Williamson-Hall Analysis in Estimation of Lattice Strain in Nanometer-Sized ZnO Particles. *J. Theor. Appl. Phys.* **2012**, *6*, No. 6.
- (25) Li, C. C.; Yang, S.; Tsou, Y. J.; Lee, J. T.; Hsieh, C. J. Newly Designed Copolymers for Fabricating Particles with Highly Porous Architectures. *Chem. Mater.* **2016**, *28*, 6089–6095.
- (26) Lu, W.; Shao, Z.; Zhang, G.; Zhao, Y.; Yi, B. Crosslinked Poly (Vinylbenzyl Chloride) with a Macromolecular Crosslinker for Anion Exchange Membrane Fuel Cells. *J. Power Sources* **2014**, *248*, 905–914.
- (27) Medrano, J. J. A.; Aragón, F. F. H.; Leon-felix, L.; Coaquira, J. A. H.; Rodríguez, A. F. R.; et al. Evidence of Particle-Particle Interaction Quenching in Nanocomposite Based on Oleic Acid-Coated Fe₃O₄ Nanoparticles after over-Coating with Essential Oil Extracted from *Croton Cajucara Benth.* *J. Magn. Magn. Mater.* **2018**, *466*, 359–367.
- (28) Nunes, A. D. C.; Ramalho, L. S.; Souza, A. P. S.; Mendes, E. P.; Colugnati, D. B.; Zufelato, N.; Sousa, M. H.; Bakuzis, A. F.; Castro, C. H. Manganese Ferrite-Based Nanoparticles Induce Ex Vivo, but Not In Vivo, Cardiovascular Effects. *Int. J. Nanomed.* **2014**, *9*, 3299–3312.
- (29) Palomec-Garfias, A. F.; Jardim, K. V.; Sousa, M. H.; Marquez-Beltrán, C. Influence of Polyelectrolyte Chains on Surface Charge and Magnetization of Iron Oxide Nanostructures. *Colloids Surf., A* **2018**, *549*, 13–24.
- (30) Gomes, J. A.; Sousa, M. H.; Da Silva, G. J.; Tourinho, F. A.; Mestnik-Filho, J.; Itri, R.; Azevedo, G. D. M.; Depeyrot, J. Cation Distribution in Copper Ferrite Nanoparticles of Ferrofluids: A Synchrotron XRD and EXAFS Investigation. *J. Magn. Magn. Mater.* **2006**, *300*, e213–e216.
- (31) Sousa, E. C.; Alves, C. R.; Aquino, R.; Sousa, M. H.; Goya, G. F.; Rechenberg, H. R.; Tourinho, F. A.; Depeyrot, J. Experimental Evidence of Surface Effects in the Magnetic Dynamics Behavior of Ferrite Nanoparticles. *J. Magn. Magn. Mater.* **2005**, *289*, 118–121.
- (32) Sousa, E. G.; Sousa, M. H.; Goya, G. F.; Rechenberg, H. R.; Lara, M. C. F. L.; Tourinho, F. A.; Depeyrot, J. Enhanced Surface Anisotropy Evidenced by Mössbauer Spectroscopy in Nickel Ferrite Nanoparticles. *J. Magn. Magn. Mater.* **2004**, *272–276*, E1215–E1217.

(33) Jardim, K. V.; Palomec-Garfias, A. F.; Andrade, B. Y. G.; Chaker, J. A.; Bão, S. N.; Márquez-Beltrán, C.; Moya, S. E.; Parize, A. L.; Sousa, M. H. Novel Magneto-Responsive Nanoplatforms Based on MnFe_2O_4 Nanoparticles Layer-by-Layer Functionalized with Chitosan and Sodium Alginate for Magnetic Controlled Release of Curcumin. *Mater. Sci. Eng., C* **2018**, *92*, 184–195.

(34) Bronstein, L. M.; Huang, X.; Retrum, J.; Schmucker, A.; Pink, M.; Stein, B. D.; Dragnea, B. Influence of Iron Oleate Complex Structure on Iron Oxide Nanoparticle Formation. *Chem. Mater.* **2007**, *19*, 3624–3632.

(35) Darwish, M. S. A.; Peuker, U.; Kunz, U.; Turek, T. Bi-Layered Polymer-Magnetite Core/Shell Particles: Synthesis and Characterization. *J. Mater. Sci.* **2011**, *46*, 2123–2134.

(36) Zhang, W.; Stolojan, V.; Silva, S. R. P.; Wu, C. W. Raman, EELS and XPS Studies of Maghemite Decorated Multi-Walled Carbon Nanotubes. *Spectrochim. Acta, Part A* **2014**, *121*, 715–718.

(37) Zhang, L.; He, R.; Gu, H. C. Oleic Acid Coating on the Monodisperse Magnetite Nanoparticles. *Appl. Surf. Sci.* **2006**, *253*, 2611–2617.

(38) Cuenca, J. A.; Bugler, K.; Taylor, S.; Morgan, D.; Williams, P.; Bauer, J.; Porch, A. Study of the Magnetite to Maghemite Transition Using Microwave Permittivity and Permeability Measurements. *J. Phys. Condens. Matter* **2016**, *28*, No. 106002.

(39) Andrianov, K. A.; Volkova, L. M. Reactions of (Chloromethyl) Ethoxysilanes with Amines. *Bull. Acad. Sci. USSR, Div. Chem. Sci.* **1959**, *8*, 255–259.

(40) Lapwanit, S.; Trakulsujaritchok, T.; Nongkhai, P. N. Chelating Magnetic Copolymer Composite Modified by Click Reaction for Removal of Heavy Metal Ions from Aqueous Solution. *Chem. Eng. J.* **2016**, *289*, 286–295.